Keratitis-Ichthyosis-Deafness Syndrome-Associated Cx26 Mutants Produce Nonfunctional Gap Junctions but Hyperactive Hemichannels When Co-Expressed With Wild Type Cx43

Isaac E. García[1], Jaime Maripillán[1], Oscar Jara[1], Ricardo Ceriani[1], Angelina Palacios-Muñoz[1], Jayalakshmi Ramachandran[2], Pablo Olivero[3], Tomas Perez-Acle[1,4], Carlos González[1], Juan C. Sáez[1,5], Jorge E. Contreras[2] and Agustín D. Martínez[1]

Mutations in *Cx26* gene are found in most cases of human genetic deafness. Some mutations produce syndromic deafness associated with skin disorders, like the Keratitis-Ichthyosis-Deafness syndrome (KID). Because in the human skin connexin 26 (Cx26) is co-expressed with other connexins, like Cx43 and Cx30, and as the KID syndrome is inherited as autosomal dominant condition, it is possible that KID mutations change the way Cx26 interacts with other co-expressed connexins. Indeed, some Cx26 syndromic mutations showed gap junction dominant negative effect when co-expressed with wild-type connexins, including Cx26 and Cx43. The nature of these interactions and the consequences on hemichannels and gap junction channel (GJC) functions remain unknown. In this study, we demonstrate that syndromic mutations, at the N terminus segment of Cx26, change connexin oligomerization compatibility, allowing aberrant interactions with Cx43. Strikingly, heteromeric oligomer formed by Cx43/Cx26 (syndromic mutants) shows exacerbated hemichannel activity but nonfunctional GJCs; this also occurs for those Cx26 KID mutants that do not show functional homomeric hemichannels. Heterologous expression of these hyperactive heteromeric hemichannels increases cell membrane permeability, favoring ATP release and Ca^{2+} overload. The functional paradox produced by oligomerization of Cx43 and Cx26 KID mutants could underlie the severe syndromic phenotype in human skin.

Journal of Investigative Dermatology (2015) **135,** 1338–1347; doi:10.1038/jid.2015.20; published online 26 February 2015

INTRODUCTION

Gap junction channels (GJCs) allow metabolic and electrical coupling between adjacent cells and are formed by the oligomerization of connexin (Cx) protein subunits. Cxs oligomerize to form hexamers called hemichannels (HCs), which reach the appositional plasma membrane and dock with other complementary HCs provided by an adjacent cell to form gap junction plaques (Segretain and Falk, 2004). In non-appositional plasma membrane, HCs connect the cytoplasm with the external milieu, allowing paracrine and autocrine signaling mediated by ATP and Ca^{2+}, among others (Stout *et al.*, 2004; Sáez *et al.*, 2005). HCs can be homomeric, if all subunits are the same Cxs or heteromeric if they are formed by two or more different Cxs; however, some Cxs are incompatible to form heteromeric channels, like Cx26 and Cx43 (Gemel *et al.*, 2004; Martínez *et al.*, 2011; Jara *et al.*, 2012). Indeed, heteromeric channels have different functional properties compared with homomeric channels; therefore, regulation of Cx–Cx interaction could be important in controlling intercellular communication (Martínez *et al.*, 2002; Martinez *et al.*, 2011; Jara *et al.*, 2012).

Mutations in the human Cx26 gene account for about 50% of genetic deafness. To date, more than 100 Cx26 mutations have been identified, but only 16 of them, mainly located at the N terminus and the transition between the first transmembrane segment and the extracellular loop segment, cause the syndromic phenotype (Martínez *et al.*, 2009). Although syndromic Cx26 mutations are sparse, they have an autosomal dominant inheritance pattern that affects proliferation and

[1]*Laboratorio de Conexinas y Panexinas, Centro Interdisciplinario de Neurociencias de Valparaíso, Facultad de Ciencias, Universidad de Valparaíso, Valparaíso, Chile;* [2] *Department of Pharmacology and Physiology, New Jersey Medical School, Rutgers University, Newark, New Jersey, USA;* [3]*Centro de Investigaciones Biomédicas, Facultad de Medicina, Universidad de Valparaíso, Valparaíso, Chile;* [4] *Fundación Ciencia and Vida, Santiago, Chile and* [5]*Departamento de Fisiología, Pontificia Universidad Católica de Chile, Santiago, Chile*

Correspondence: Agustín D. Martínez, Laboratorio de Conexinas y Panexinas, Centro Interdisciplinario de Neurociencias de Valparaíso, Facultad de Ciencias, Universidad de Valparaíso, Avenida Gran Bretaña 1111, Playa Ancha, Valparaíso, Chile. E-mail: agustin.martinez@uv.cl

Abbreviations: CX, connexin; DCF-HBSS, divalent cation-free Hanks' balanced salt solution; GFP, green fluorescent protein; GJC, gap junction channels; HC, hemichannel; hCx26, human Cx26; KID, Keratitis-Ichthyosis-Deafness syndrome

Received 12 August 2014; revised 13 January 2015; accepted 14 January 2015; accepted article preview online 27 January 2015; published online 26 February 2015

differentiation of skin keratinocytes and produces progressive corneal neovascularization and hair and nail dystrophies like in the Keratitis-Ichthyosis-Deafness (KID) syndrome (Cáceres-Ríos *et al.*, 1996; Kelsell *et al.*, 2000; Arita *et al.*, 2006). It is hypothesized that syndromic mutations produced gain-of-function HCs (Gerido *et al.*, 2007; Lee *et al.*, 2009; Sánchez *et al.*, 2010; Levit *et al.*, 2012). However, some syndromic mutations, like Cx26S17F, lead to nonfunctional HCs, but they still developed a severe KID syndrome phenotype (Richard *et al.*, 2002; Mazereeuw-Hautier *et al.*, 2007; Lee *et al.*, 2009). Most of these studies have been performed in homomeric HCs, which may not reproduce what occurs in the disease. In human skin, Cx26 is co-expressed with Cx43, Cx30, and Cx31 (Salomon *et al.*, 1994); as the KID syndrome is inherited as autosomal dominant condition, it is possible that KID mutations change the interaction and functional properties of Cx26 with other Cxs. Thus, to better understand the disease mechanisms, it is necessary to investigate the effect of Cx26 KID mutations when co-expressed with other Cxs found in the human skin.

Here, we functionally analyzed several N terminus Cx26 mutants that were co-expressed, or not, with wild-type Cx26 and Cx43. We focused on N14Y and S17F syndromic mutations, as well as two mutations located at residue 12 that can cause syndromic (G12R) or non-syndromic (G12V) deafness. The residue G12 is located inside the pore at the plasma membrane level (Maeda *et al.*, 2009; Kwon *et al.*, 2011), whereas residues N14 and S17 face the cytoplasm in the hinge region of the Cx26 N terminus (Figure 1a1). The effect of two non-syndromic mutations, V37I and A40G, positioned at the TM1/ECL1 transition, was also assessed to compare interactions with wild-type Cx26 and Cx43.

RESULTS

Non-syndromic and syndromic mutations located at the N terminus segment of Cx26 reduce or eliminate GJC formation and/or function

To assess the effect of Cx26 mutations on traffic, oligomerization, and functional state of GJCs, HeLa cells were transfected with wild-type Cx26 (Cx26 hereinafter) or deafness mutants attached to green fluorescent protein (GFP) to visualize their subcellular localization. All transfections were performed in a HeLa parental cell line that either does not express Cx26 and Cx43 (Supplementary Figure S1a online) or does not show GJC currents (Supplementary Table S1 online), confirming that this cell line is Cx-expression deficient. In contrast, we observed large GJ plaques in HeLa cells expressing Cx43, Cx26 (Supplementary Figure S1b online), Cx26-GFP or the non-syndromic Cx26G12V-GFP mutant (Figure 1a2,3) similar to that previously reported for non-syndromic mutants Cx26V37I and Cx26A40G (Jara *et al.*, 2012). Conversely, syndromic mutants formed few GJ plaques, suggesting intracellular trapping or preferential localization in non-appositional plasma membrane (Figure 1a4–6 and b).

We next evaluated the functional state of GJCs formed by homomeric mutations at the N terminus. Dye-transfer and transjunctional conductance (g_j), between cells expressing syndromic or non-syndromic mutants, were indistinguishable from those obtained in untransfected cells (Supplementary Table S1 online). Thus, these mutations completely abolished the formation of functional GJCs.

Syndromic N terminus mutations affect Cx26 oligomerization

Diffuse cytoplasmic and/or perinuclear localizations (Figure 1a4–6) identified for syndromic mutants may reflect partial intracellular trapping because of defective protein oligomerization. This possibility was analyzed by velocity sedimentation assays in sucrose gradients. We found that the oligomeric and monomeric fractions of Cx26-GFP, Cx26G12V-GFP, and Cx26G12R-GFP present similar sedimentation patterns to Cx26 (Figure 1c–f), which was consistent with those reported previously (Gemel *et al.*, 2004; Jara *et al.*, 2012). However, for syndromic mutants Cx26N14Y-GFP and Cx26S17F-GFP (Figure 1g–h), their oligomeric fractions shifted to lower sucrose densities, suggesting the formation of intermediate arrangements with fewer hexamers.

To identify a potential dominant negative effect of Cx26 mutants on Cx26 GJC function, we co-expressed the GFP-tagged mutants with Cx26 containing a hemagglutinin (HA) tag (Cx26-HA). In these cells, all mutants co-localized with Cx26-HA and formed abundant and large GJ plaques between pairs of co-expressing cells (Supplementary Figure S2a–f online), suggesting that Cx26 rescues the traffic and delivery of syndromic mutants to appositional areas. Interestingly, all N terminus mutants, either syndromic or non-syndromic, were not negative dominant of Cx26 GJCs. Nevertheless, we cannot rule out subtle changes in the channel permeability, as we found that GJCs formed by Cx26 and either syndromic mutant Cx26N14Y or Cx26S17F showed reduced coupling to Lucifer yellow (-2), but normal coupling to the smaller permeability tracer neurobiotin ($+1$; Supplementary Table S1 online), suggesting that these channels are less permeable to negatively charged molecules and/or they have a reduce pore size.

Syndromic mutations in the N terminus change the oligomerization compatibility of Cx26

Although Cx26 is co-expressed with Cx43 in cochlear cells (Forge *et al.*, 2003) and skin keratinocytes (Salomon *et al.*, 1994; Richard, 2000; Beyer *et al.*, 2001; Richard *et al.*, 2002; Arita *et al.*, 2006), they are incompatible to form heteromeric channels (Gemel *et al.*, 2004). Hence, we aim to study whether oligomerization of these incompatible Cxs results in compatible interactions as consequence of syndromic mutations located at the N terminus of Cx26. HeLa cells expressing Cx43 were transiently transfected with Cx26-GFP or mutants. We found that Cx43 and Cx26-GFP localize at the same plaques, but segregate in different regions (Figure 2a1–4), which is consistent with their oligomerization incompatibility (Gemel *et al.*, 2004). No co-localization was observed between Cx43 and the non-syndromic mutants Cx26G12V-GFP (Figure 2a5–8), Cx26V37I-GFP, or Cx26A40G-GFP (Supplementary Figure S3 online). However, all syndromic mutants perfectly co-localized with Cx43 in intracellular compartments and in GJ plaques (Figure 2a9–20), suggesting the formation of heteromeric channels. Consistently, Cx sedimentation analysis showed that only co-expression of

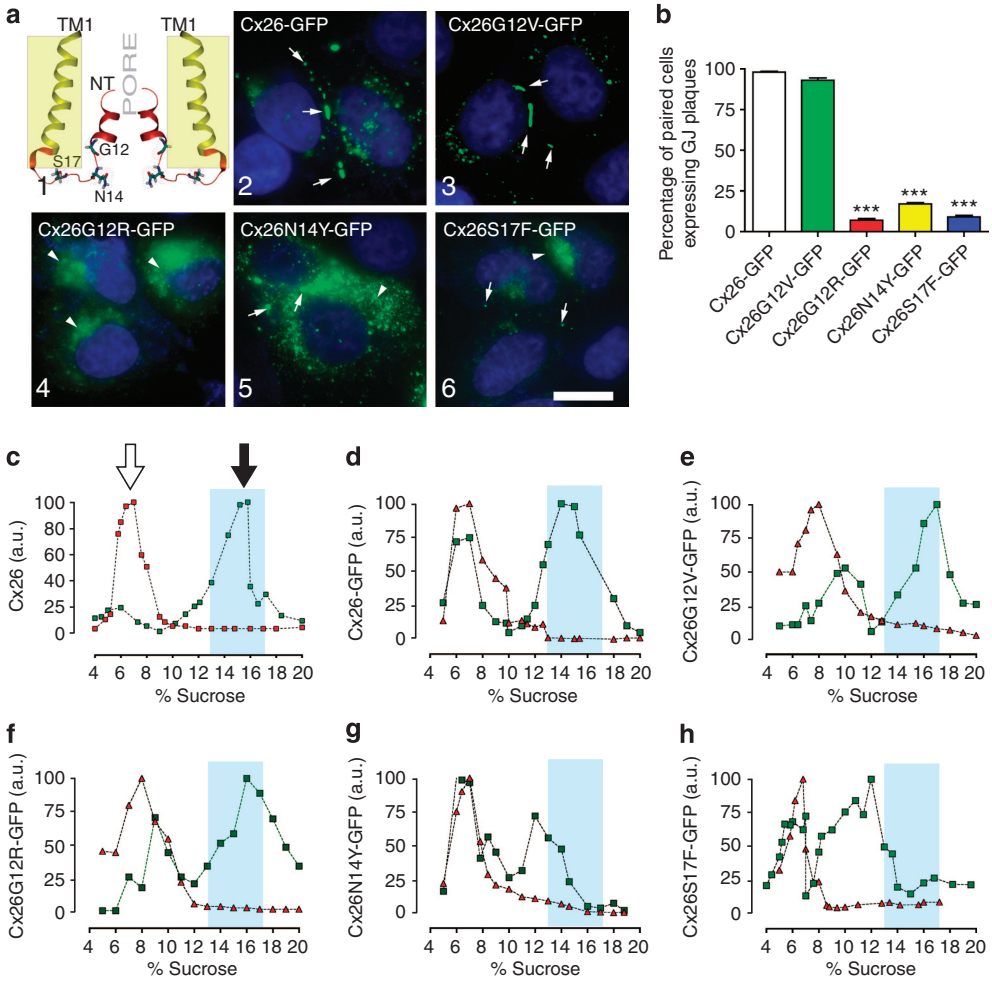

Figure 1. Syndromic mutations reduce or eliminate gap junction channel (GJC) formation. (**a1**) TM1 and NT of two Cx26 subunits with highlighted residues at the NT that are linked to deafness mutations. Yellowish rectangle indicates plasma membrane region. (**a2–6**) Confocal images show the respective subcellular localization of cells expressing Cx26 wild-type or mutants. White arrows indicate GJ plaques. Arrowheads indicate perinuclear labeling. Bar = 15 μm. (**b**) Percentage of paired cells expressing GJ plaques per condition. (***$P<0.001$; $n=5$, 250 paired cells for condition). (**c–h**) Syndromic mutations, N14Y and S17F, affect oligomerization. Graphs represent the sedimentation profile of monomer and oligomers (in arbitrary units of Cx amount; a.u.) of WT or mutants Cx26. SDS treated fractions (red triangles). Black-filled arrows in (**c**) show the hexameric peak, and the unfilled arrows show monomeric peaks. Light blue columns indicate where WT Cx26 hexamers sedimented ($n=4$). Cx, connexin; GFP, green Fluorescent Protein; GJC, gap junction channel; WT, wild type.

Cx43 with any syndromic mutant (Figure 2e–g) promoted a shift in the sedimentation profiles of both proteins to overlap in a new oligomeric peak, which varied depending on the protein pair analyzed, confirming the formation of heteromeric channels between Cx43 and syndromic mutants. However, these heteromeric pairs produced nonfunctional GJCs, suggesting a total transdominant-negative effect of the syndromic mutants on Cx43 GJCs (Supplementary Table S1 online). To rule out that the null GJCs observed under previous conditions were not consequences of mutant Cx26 overexpression with respect to Cx43, we did transient transfections using different ratios of plasmid complementary DNAs carrying Cx43-RFP and Cx26-GFP or its mutant variants (1:1 and 1:0.3 ratios, respectively) and then quantified the fluorescence for each fluorescent protein to demonstrate the relative reduction in the expression levels of each mutant Cx26 (Supplementary Figure S4 online). Regardless of the ratio, we did not observe any junctional coupling in cells co-expressing Cx43-RFP with any Cx26 syndromic mutant (Supplementary Table S3 online). Although we cannot estimate the molecular stoichiometry, our experiments suggest that the negative dominant effect of syndromic mutant over Cx43 GJC is strong. In addition, a previous report by Rouan and colleagues also showed that Cx26 with a syndromic mutation in TM1/EL1 is a negative dominant of Cx43 GJCs (Rouan *et al.*, 2001), suggesting that interaction with Cx43 would be a general feature of syndromic Cx26 mutants.

Syndromic mutations G12R and N14Y, but not S17F, produce homomeric HCs with gain of function

Because syndromic mutations are linked to gain in HC function, we performed YO-PRO uptake assays to address HC function. Under physiological extracellular Ca^{2+} concentration, HCs are preferentially closed; however, cells that

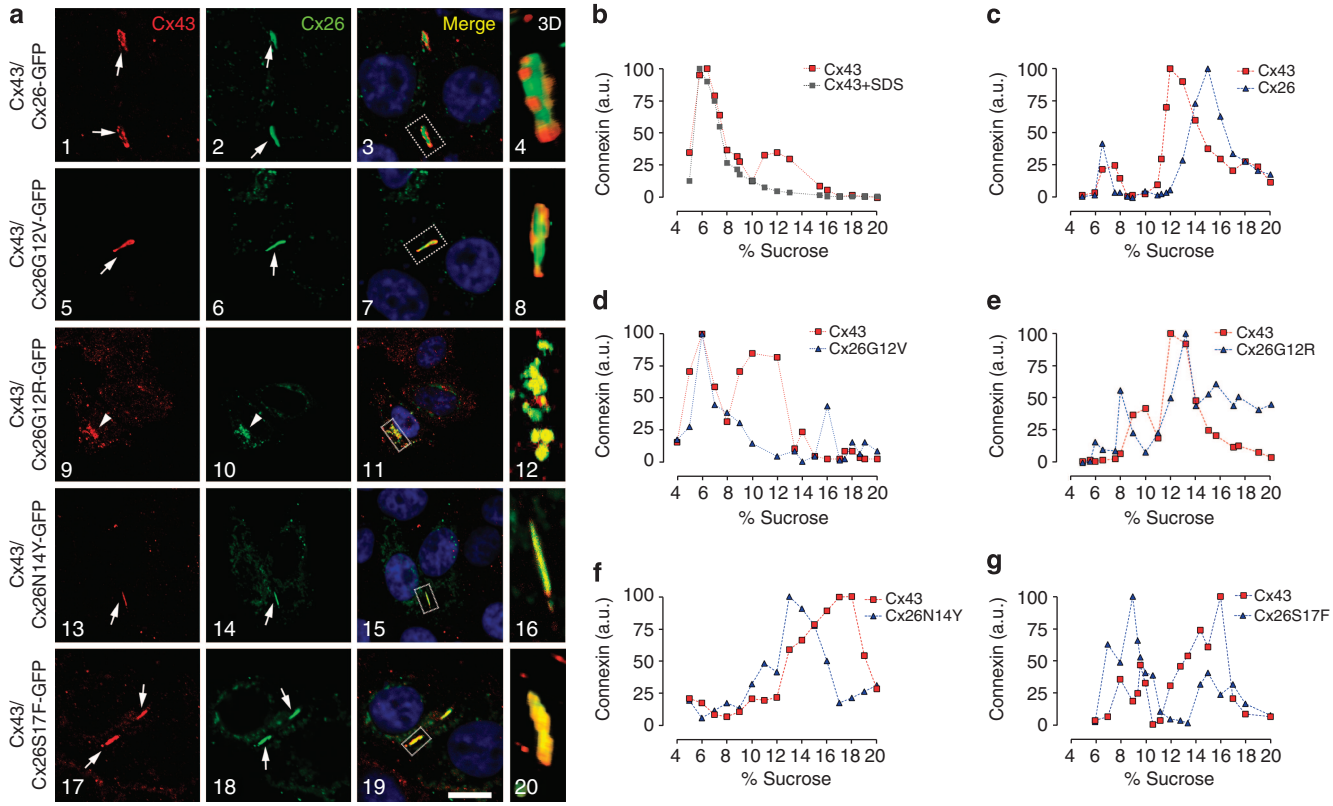

Figure 2. Syndromic mutations change the oligomerization compatibility of Cx26. (**a**) Confocal images of HeLa cells co-expressing Cx43 (red labeling) with WT or mutants Cx26. Arrows point GJ plaques. Arrowheads show perinuclear staining. Nuclei were staining with 4′,6-diamidino-2-phenylindole (DAPI). Dashed rectangles in the merged panels show regions of interest for three-dimensional image projections. Bar = 10 μm. (**b**, **c**) Cx43 and Cx26-GFP do not co-sediment in the same oligomeric fractions. Graphs represent the levels of Cx43 and Cx26-GFP in each sucrose fractions in samples from HeLa cells that were transfected with Cx43 (**b**) or co-transfected with Cx43 and Cx26-GFP (**c**). In (**b**) samples were treated with SDS (gray square) to reveal Cx43 monomers. (**d**–**g**) Syndromic mutants co-sediment with Cx43 in new oligomeric fractions. Graphs show levels of Cx43 and mutant Cx26 in sucrose gradient fractions from cells co-transfected with Cx43 and the respective mutant ($n = 4$). Cx, connexin; GFP, green fluorescent protein; GJ, gap junction; WT, wild type.

expressed the syndromic mutants Cx26G12R-GFP or Cx26N14Y-GFP showed uptake rates that were ~10 and ~4 times greater compared with what was observed in cells expressing Cx26-GFP, respectively, suggesting that both mutants increased the activity of homomeric HCs enhancing permeation to positively (+2) charged molecules (Figure 3b–c). This result is consistent with previous reports, indicating that Cx26G12R mutation produces high HC activity in the presence of physiological extracellular Ca^{2+} concentrations (Lee *et al.*, 2009). To further examine the presence of HCs in the cell membrane, dye uptake was evaluated in divalent cation-free Hanks' balanced salt solution (DCF-HBSS), which enhances HC activity, or in the presence of the lanthanum ions (La^{3+}), a widely used HC blocker (Figure 3a). In this condition, YO-PRO uptake was significantly increased in cells that expressed Cx26 or all the mutants, except for Cx26S17F-GFP (Figure 3a and d). Conversely, YO-PRO uptake was partially or completely reduced in the presence of La^{3+} in wild-type and mutant HCs (Figure 3a). The variation in YO-PRO uptake was neither related to differences in expression levels (Supplementary Figure S1c online) nor depended on the expression levels of the mutants as revealed by the correlation analysis of the relative-uptake rate/GFP-expression ratio (Supplementary Figure S5a online).

A significant increase in YO-PRO uptake under normal extracellular Ca^{2+} concentration was recorded in cells that co-expressed Cx26 with Cx26G12R-GFP or Cx26S17F-GFP. Such increase was several times greater when compared with their respective homomeric counterparts or cells co-expressing Cx26 and Cx26-GFP (Figure 3e–h). Nevertheless, HCs composed by Cx26 and Cx26G12V-GFP or syndromic Cx26N14Y-GFP were less active compared with their respective homomeric conformations and Cx26/Cx26-GFP HCs, which would reflect the formation of inactive HCs. Correlation analysis indicates that levels of YO-PRO uptake observed were not related to differences in expression levels (Supplementary Figure S5b online).

Syndromic mutants form hyperactive heteromeric HCs with Cx43

We found no significant difference in YO-PRO uptake in cells co-expressing Cx43 with Cx26-GFP or with non-syndromic mutants Cx26G12V-GFP (Figure 3j–k), Cx26V37I-GFP, or Cx26A40G-GFP (Supplementary Figure S3c online). In

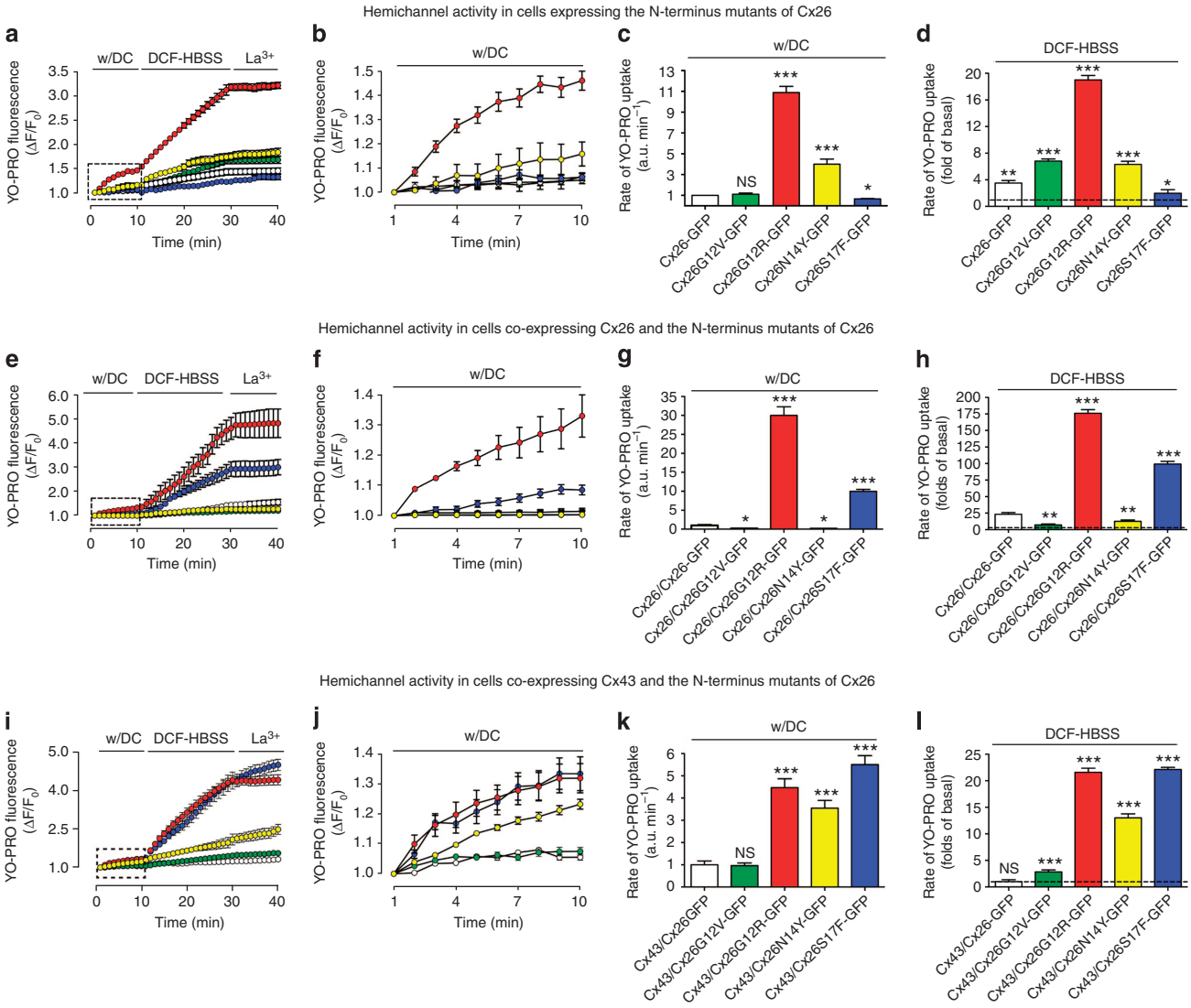

Figure 3. All syndromic mutants form hyperactive heteromeric hemichannels (HCs) with Cx43. The functional state of HCs was determined in time-lapse experiments of YO-PRO uptake by HeLa cells expressing Cx26-GFP (open symbols), Cx26G12V-GFP (green), Cx26G12R-GFP (red), Cx26N14Y-GFP (yellow), or Cx26S17F-GFP (blue; **a**–**d**) or by cells co-expressing these constructs with WT Cx26 (**e**–**h**) or Cx43 (**i**–**l**). (**a**, **e**, **i**) Uptake under physiological extracellular divalent cation concentrations (w/DC) for 10 minutes, followed by a 20 minutes bath in Ca^{2+}/Mg^{2+} free (DCF-HBSS). Then, 100 μM La^{3+} was added to block HCs. (**b**, **f**, **j**) Magnification of the area indicated by the rectangle in the graph (**a**, **e**, **i**). (**c**, **d**; **g**, **h**; **k**, **l**) The rate of uptake was determined calculating the uptake slope in cells bathed with physiological (**c**, **g**, **k**) or DCF-HBSS (**d**, **h**, **l**) solution. Data are presented as average ± SEM ($n = 7$). *t*-Test for unpaired data. ***$P < 0.001$; **$P < 0.01$; *$P < 0.05$. Cx, connexin; HC, hemichannel; DCF-HBSS, divalent cation-free Hanks' balanced salt solution; GFP, green fluorescent protein; WT, wild type.

contrast, uptake mediated by heteromeric HCs formed by all syndromic mutants with Cx43 showed higher uptake, even in the presence of divalent cations (Figure 3j–k), which was boosted after the removal of extracellular Ca^{2+} (Figure 3i and l), suggesting that these heteromeric HCs are still sensitive to Ca^{2+}. The effects described here were not a consequence of different expression levels of Cx26 mutants, because they were observed even in cells that express low levels of syndromic mutant Cxs (Supplementary Figure S5c online).

To unequivocally assess those Cx26 mutations that increase HC activity when forming homomeric and heteromeric HCs, we performed electrophysiological studies using the two-electrode voltage clamp technique. Macroscopic currents were elicited by depolarizing pulses in *Xenopus laevis* oocytes expressing homomeric and heteromeric HCs, to examine the current–voltage relationship. Consistent with previous reports (White *et al.*, 1999; Hansen *et al.*, 2014), oocytes expressing human Cx43 did not exhibit detectable HC macroscopic currents (Figure 4a). The lack of HC currents was also observed in oocytes expressing Cx26G12V, Cx26N14Y, or Cx26S17F alone (Supplementary Figure S6 online). To evaluate heteromeric HC currents, equal amounts of complementary RNA were co-injected in oocytes to obtain 1:1 protein expression ratios. Co-expression of Cx43 with the non-syndromic G12V mutant did not elicit HC currents (Figure 4c and g), supporting our previous interpretation that these proteins

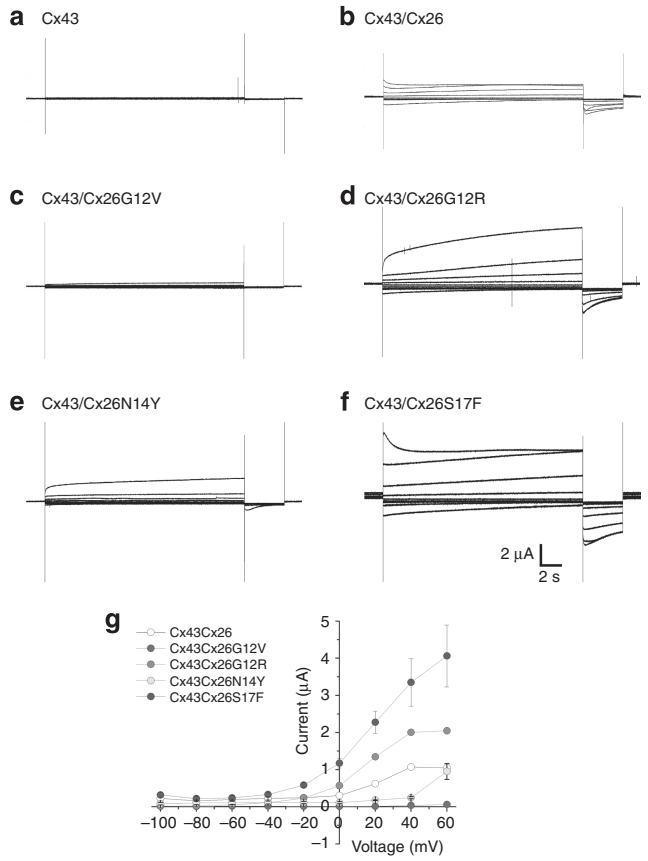

Figure 4. Heteromeric hemichannels (HCs) composed of Cx43 and the syndromic mutants produce large macroscopic currents. Membrane currents from oocytes expressing Cx43 alone or Cx43 with Cx26 mutants were recorded using the two-electrode voltage clamp technique. HC currents were activated in response to depolarizing voltage steps from a holding potential of −10 mV and stepped in 20 mV increments from −100 mV to +60 mV. Representative currents traces are showed for hCx43 alone (**a**) or for hCx43 co-expressed with wild-type Cx26 (**b**), hCx26G12V (**c**), hCx26G12R (**d**), hCx26N14Y (**e**), or hCx26S17F (**f**). (**g**) Graphic depicted the macroscopic current–voltage relationship of heteromeric HCs. The data represent mean ± SEM of at least five independent experiments. Cx, connexin; HC, hemichannel; hCx43, human Cx43.

do not interact. Conversely, co-expression of Cx43 with the syndromic Cx26G12R and Cx26S17F mutants promotes larger HC currents (Figure 4d and f). Lower HC currents were detected in oocytes co-expressing Cx43 and the Cx26N14Y mutant (Figure 4e); yet, they were significantly larger at high positive potentials (>50 mV) compared with those observed for oocytes expressing Cx43 or Cx26N14Y alone. Co-expression of Cx26 and Cx43 showed HC currents with similar kinetic to those previously described for Cx26 alone (Lopez *et al.*, 2013a, 2013b).

Expression of heteromeric channels formed by Cx26 syndromic mutants and Cx43 promotes intracellular Ca^{2+} overload and ATP release

Compelling evidence has indicated the existence of a strong relationship between HC activity and increments in intracellular Ca^{2+} concentration and ATP release (Stout *et al.*, 2002; Saez *et al.*, 2010; Fiori *et al.*, 2012), both are important for normal functioning of the cochlea and the skin (Djalilian *et al.*, 2006; Anselmi *et al.*, 2008). To determinate changes in basal cytosolic Ca^{2+} levels from HeLa cells expressing homomeric and heteromeric HCs, cells loaded with the non-ratiometric probe Fura-Red were incubated in normal extracellular solution. Only cells that co-expressed Cx43 with syndromic mutants showed higher intracellular Ca^{2+} signal, which was almost saturated as indicated by treating these cells with 10 μM ionomycin that only produced a minor increase in the Ca^{2+} signal (Figure 5a and b). Because Fura-Red has very limited sensitivity to Ca^{2+} concentration (above 1 μM), we also used Indo-1AM to more accurately estimate changes in the intracellular Ca^{2+} concentration among different mutants. HeLa cells expressing homomeric HCs, formed by Cx26G12R or Cx26N14Y mutants, but not Cx26S17F, exhibit higher levels of intracellular Ca^{2+} when compared with HeLa cells expressing homomeric wild-type Cx26 (Supplementary Figure S7 online). Consistently with the Ca^{2+} overload reported by the Fura-Red experiments, cells co-expressing Cx43 with any syndromic mutants showed elevated intracellular Ca^{2+} concentration. In particular, cells co-expressing Cx43 and Cx26S17F display intracellular Ca^{2+} levels almost twofolds compared with those measured in cells co-expressing the wild-type counterparts (Figure 5c).

Because extracellular ATP release correlates with HC activity (Stout *et al.*, 2002), we explore the basal HC-dependent ATP release. As expected for hyperactive HCs, we found more ATP release from cells expressing heteromeric HCs formed by Cx43 with any syndromic Cx26 mutants (Figure 5d).

DISCUSSION

In the present work, we propose a possible molecular mechanism that might underlie the severity of the KID syndrome by mutations at the N terminus segment of Cx26. We demonstrate that Cx26 syndromic mutations produce aberrant Cx–Cx interactions leading to the formation of heteromeric HCs and GJCs with Cx43. These heteromeric HCs, but not GJCs, present exacerbate activity (gain in function) that may lead to dysfunction of paracrine signaling and Ca^{2+} overload (Figure 5; Supplementary Table S4 online). Although KID syndromic mutations have been previously associated with hyperactive HCs, some syndromic mutations formed inactive homomeric HCs contradicting the previous mechanistic explanation for the disease. Because both, Cx26 and Cx43, are highly expressed in the human skin (Salomon *et al.*, 1994), we propose that all syndromic mutations at the N terminus could produce the functional paradox of hyperactive heteromeric HCs (Cx43/Cx26 mutants), but nonfunctional GJCs (Supplementary Table S4 online), which can worsen the skin damage in patients carrying these mutations (Mazereeuw-Hautier *et al.*, 2007).

At the molecular level, our data demonstrate a critical role of the N terminus in controlling Cx oligomerization. We found that mutations facing the cytoplasmic environment (i.e., Cx26N14Y and Cx26S17F) disrupt the proper formation of

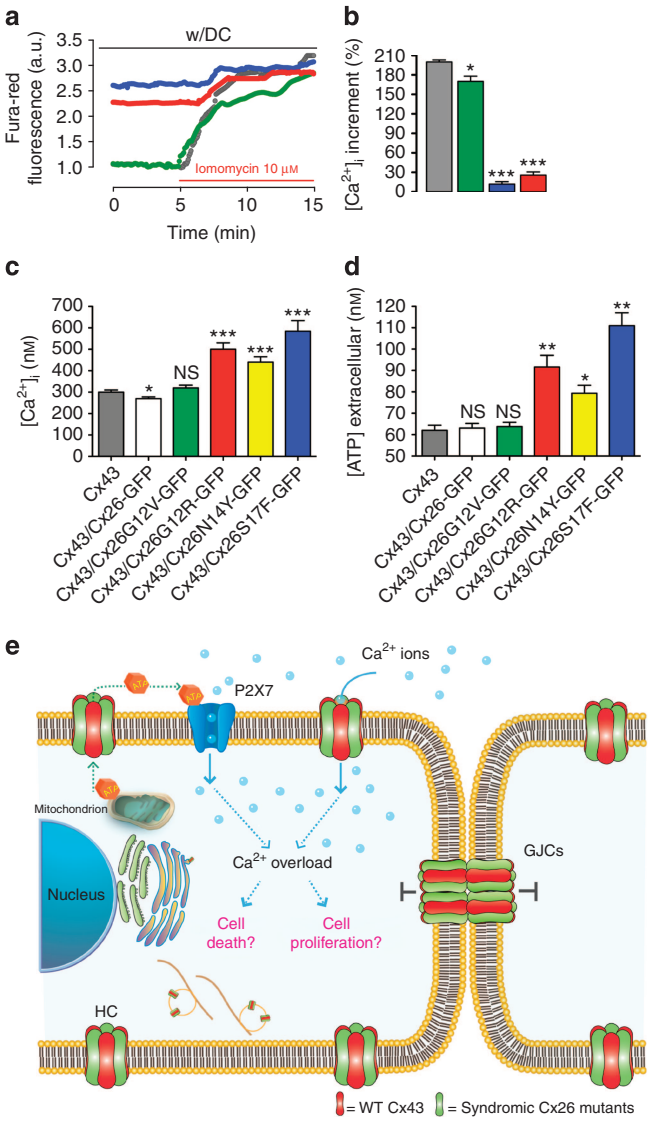

Figure 5. Heteromeric hemichannels formed by syndromic mutants and Cx43 promote cellular Ca^{2+} overload and ATP release. (**a**) Time course of Ca^{2+} signal obtained with probe Fura-Red in cells expressing Cx43 (gray), or co-expressing Cx43 with non-syndromic Cx26G12V-GFP (green), or syndromic Cx26G12R-GFP (red) and Cx26S17F-GFP (blue) before and after application of the Ca^{2+} ionophore ionomycin (100 μM). (**b**) Percentage of the Ca^{2+} signal increments induced by ionomycin. (**c**) Intracellular Ca^{2+} concentration in HeLa cells or in cells expressing Cx43 or co-expressing Cx43 with Cx26-GFP or Cx26S17F-GFP. (**d**) Measurement of ATP release during 10 min of cellular incubation of HeLa cells co-expressing Cx43 with the N terminus mutants. Data are presented as average ± SEM ($n = 20$). *t*-Test for unpaired data. ***$P < 0.001$; **$P < 0.01$; *$P < 0.05$ (**e**) Model of cell signaling induced by expression of aberrant heteromeric HCs but nonfunctional GJCs in the KID syndrome. Cx, connexin; GFP, green fluorescent protein; GJC, gap junction channel; HC, hemichannel; KID, Keratitis-Ichthyosis-Deafness syndrome.

hexamers but still allow the formation of intermediate Cx oligomers (Figure 1g and h). The latter is consistent with the formation of Cx26 dimers that depend on TM1 (Jara *et al.*, 2012) as the first step into the oligomerization process. However, mutations in the N terminus might affect subsequent steps in hexamer formation, like the check point for oligomerization compatibility between Cxs. Our results support the idea that such check point is located in the Cx26 N terminus, as it has been previously suggested for this Cx (Lagree *et al.*, 2003; Martínez *et al.*, 2009; Jara *et al.*, 2012) and for acetylcholine receptors (Verrall and Hall, 1992). These results are consistent with the notion that an intact N terminus is critical for the formation (Kyle *et al.*, 2008) and proper functioning of GJCs, as this segment is part of the transjunctional voltage sensor (Verselis *et al.*, 1994) and gating mechanism (Barrio *et al.*, 1991; Maeda *et al.*, 2009; Bargiello *et al.*, 2012).

Consistent with previous studies (Lee *et al.*, 2009) and with the YO-PRO uptake experiments, we observed that *Xenopus* oocytes expressing homomeric Cx26S17F mutants do not display HC currents upon membrane depolarization. Suggesting that this mutation drastically decreases the open probability and/or ionic conductance in homomeric HCs. Similarly, Cx43 when expressed in *Xenopus* oocytes does not show macroscopic HC currents, but it does allow uptake of ethidium bromide (Hansen *et al.*, 2014). Only few single Cx43 HCs with very low open probability have been detected in the whole-cell configuration from cells expressing high levels of Cx43 proteins at the plasma membrane (Contreras *et al.*, 2003); yet, significant dye uptake is observed over larger periods of time-video recording (Sáez *et al.*, 2005; Sáez *et al.*, 2010). Remarkably, we showed that the co-expression of Cx43 and Cx26S17F results in large HC currents (Figure 4f), which can only be explained by formation of heteromeric HCs between these two Cxs, as supported by co-localization and velocity sedimentation assays. Similar results were found when Cx26N14Y and Cx26G12R were co-expressed with Cx43. Conversely, the non-syndromic mutant Cx26G12V did not show significant levels of HC currents or dye uptake when co-expressed with Cx43, consistently with the biochemical data showing that this mutation does not lead to the formation of heteromeric HCs with Cx43, but it does interact with wild-type Cx26, without the formation of hyperactive functional HCs. Similar results were observed for non-syndromic mutants Cx26V37I and Cx26A40G.

In the KID syndrome several tissues are affected, but the most extensive damage is observed at the epidermis, a tissue in which Cx26 and Cx43 are the main Cxs expressed (Goliger and Paul, 1994; Salomon *et al.*, 1994; Wiszniewski *et al.*, 2000), playing a critical role in keratinocytes homeostasis maintenance and migration from the basal to the cornified layer (Risek *et al.*, 1992). Overexpression and ectopic expression of Cx26 are associated with psoriatic plaques and ATP release, delayed epidermal barrier recovery, and inflammatory responses (Djalilian *et al.*, 2006). In addition, a KID patient carrying mutation N14Y present also ectopic skin expression of Cx26 that co-localized with Cx43 (Arita *et al.*, 2006). In addition, P2X purinergic receptors are expressed in the skin and ATP signaling is important for differentiation and proliferative processes in keratinocytes, as well as hyperplasia induced after skin barrier disruption (Denda *et al.*, 2002). Our findings show that the expression of syndromic heteromeric HCs and GJCs increases basal concentrations of intracellular Ca^{2+} and ATP release, which is consistent with the notion

that both signaling agents permeate through HCs (Stout *et al.*, 2002; Fiori *et al.*, 2012). Our results support the notion that the KID syndrome involves keratinocyte homeostasis misregulation as consequences of leaky heteromeric HCs but nonfunctional GJC, which might promote ATP release, intracellular Ca^{2+} overload, and cell death and/or proliferation (Figure 5e). Hence, this study supports the idea to use HC blockers as possible therapeutic agents for this disease.

MATERIALS AND METHODS

Molecular cloning

Wild-type rat Cx26 cDNA (accession: NM_001004099) was cloned in the pcDNA3.1/CT-GFP-TOPO vector (Invitrogen, Thermo Fisher Scientific, Waltham, MA). Site-directed mutagenesis was generated using the Quick-Change II kit (Agilent Technologies; Santa Clara, CA). For some experiments Cx26 or its variants contain HA epitope tag appended to their C terminus. Primer sequences are detailed in Supplementary Table S2 online. DNA was sequenced by Macrogen (Seoul, Korea) and analyzed using the ''Vector NTI Advance'' software (Invitrogen).

Immunofluorescence

Parental HeLa cell transfection and immunofluorescence were performed as previously described (Jara *et al.*, 2012). Antibodies against Cx43, Cx26, and anti-HA were from Invitrogen. Image acquisition was performed with a Nikon Eclipse C1-Plus confocal microscope. Image processing and three-dimensional reconstruction were using the EZ-C1 and the NIS-Elements Viewer 4.0 software, respectively (Nikon Instruments, Minato-ku, Tokyo, Japan).

Velocity of sedimentation in sucrose gradients and immunoblotting

Transfected HeLa cells were harvested and lysed as indicated previously (Jara *et al.*, 2012). Soluble fractions were subjected to sedimentation velocity through 5–20% (w/v) linear sucrose gradients, as previously described (Berthoud *et al.*, 2001; Jara *et al.*, 2012). To determine the percentage of sucrose at which Cx monomers sediment, Triton X-100 soluble fractions were treated with SDS to disaggregate the oligomers. After centrifugation for 22 hours at 100,000 g, 250 µl-fractions were collected and analyzed by immunoblotting as previously described (Martinez *et al.*, 2002; Jara *et al.*, 2012).

Measurement of GJC activity

Intercellular dye-coupling was performed as previously described (Martinez *et al.*, 2002; Jara *et al.*, 2012) and visualized with a Nikon TE-2,000U inverted microscope (Nikon ACT-2U, Tokyo, Japan). The results are reported as incidence of coupling—that is, the percentage of microinjections that resulted in tracer diffusion to one or more adjacent cells. Electrophysiological recordings in pairs of HeLa cells were conducted with double whole-cell patch clamp essentially as described in (Jara *et al.*, 2012). Total gap junctional conductance (g_j) was calculated by using the formula ($g_j = I_j/[V_{j\ \text{cell}\ 1} - V_{j\ \text{cell}\ 2}]$).

Assessment of HC activity

Cells plated on glass coverslips were bathed in physiological extracellular solution containing 200 nM of YO-PRO-1 uptake (375 Dalton/+2) and subjected to dye uptake time-lapse imaging as described previously (Contreras *et al.*, 2002; Jara *et al.*, 2012). The bath solution was replaced by Ca^{2+}–Mg^{2+}-free solution (DCF-HBSS, Invitrogen) containing 200 nM YO-PRO-1, and, tracer uptake was recorded for 20 minutes, followed by the addition of 100 µM $LaCl_3$ (Sigma-Aldrich, St. Louis, MO) for an additional 10 minutes. Regions of interest were obtained with a original magnification ×40 objective in a Nikon TE-2,000U inverted microscope and captured with a Nikon DS-2WBc fast-cooled monochromatic digital camera (8-bit) every 60 seconds. Image analysis and quantification of fluorescence intensity were performed with Image J (http://rsbweb.nih.gov/ij/).

Molecular cloning and HC electrophysiology

Wild-type human Cx26 cDNA was purchased from (Origene; Rockville, MD) and was subcloned in the pGEM-HA vector (Promega; Madison, WI) for *in vitro* translation. Mutations of human Cx26 were produced with Quick-Change II Site-Directed Mutagenesis kits (Agilent Technologies). DNA sequencing performed at the New Jersey Medical School Molecular Resource Facility confirmed the amino acid substitutions. Nhe1-linearized human Cx26 wild-type, Cx43 and mutant DNAs were transcribed in vitro to cRNAs using the T7 Ultra mMessage Machine kit (Ambion, Thermo Fisher Scientific, Waltham, MA). Electrophysiological data were collected using the two-electrode voltage-clamp technique as in our previous studies (Lopez *et al.*, 2013a).

Ca^{2+} imaging

Ionomycin-induced Ca^{2+} overload was measured by imaging of Fura-Red acetoxymethylester (Invitrogen). Briefly, HeLa cells growing in coverslips were loaded with 15 µM Fura-red for 20 minutes at room temperature. Each coverslip was placed in a perfusion chamber mounted on an IX81 inverted epifluorescence microscope (Olympus, Shinjuku, Tokyo, Japan) equipped with a 40×/1.4 numerical aperture oil-immersion objective. Image analysis was performed using the Excellent Pro software. The relative fluorescence ratio was calculated by dividing fluorescence (F) at each time point by the initial fluorescence value (F_0).

Intracellular Ca^{2+} concentration was measured using Indo-1AM (Molecular Probes, Invitrogen; Thermo Fisher Scientific) based on the standard ratio method (Grynkiewicz *et al.*, 1985; Jacquemond, 1997). Briefly, HeLa cells growing in 25 mm coverslips were loaded with 5 µM Indo-1AM (dissolved in 20% pluronic acid in DMSO) for 30 minutes at 37 °C in normal extracellular solution. Each coverslip was placed in a perfusion chamber mounted on the stage of a microscope (Diaphot 200-Nikon) equipped with a photomultiplier (Micron System, MS878; NJ). Indo-1 signals were amplified with an EPC 10-USB amplifier (HeKa Electronics; Harvard Biosciences, Holliston, MA). Analog/digital signal conversion was performed with a DigiData 1,200 Series card (Axon Instruments; Molecular Devices; Sunnyvale, CA). The Patch Master program (HeKa Electronics) was used for data acquisition, and data analysis was carried out with the Igor6 software.

Extracellular ATP measurements

ATP release was assessed with the luciferin/luciferase-based ATP Determination Kit (Molecular Probes, Invitrogen). Briefly, for each condition, 50,000 cells/well were seeded in a 24-well plaque. Twenty-four hours later, the culture medium was washed out and replaced with Hanks' balanced salt solution containing 1.8 mM Ca^{2+},

and cells were incubated for 10 minutes at 37 °C. Subsequently, 5 µl samples of extracellular milieu were mixed with 45 µl ATP-mix solution in a 96-well plaque. Accumulated ATP was determined using an Appliskan Luminometer (Thermo Electro; Thermo Fisher Scientific) based on a calibration curve range from 1 nM to 1 µM ATP. Data were collected with the SkanIT software (Thermo Electro).

CONFLICT OF INTEREST

The authors state no conflict of interest.

ACKNOWLEDGMENTS

We thank Dr José Ignacio García-Palacios for substantial comments on the manuscript and Victoria Devia for technical support in confocal microscopy. This work was supported by the Fondecyt-1130855 to ADM, the Anillo ACT-1104 grant to CG and ADM, Fondecyt-1120802 to CG, Fondecyt-3150634 to IEG, CONICYT fellow and *Beca Apoyo a la realización de Tesis Doctoral* AT24121123 fellowship grant to IEG, Fondecyt-11100047 to PO, and Fondecyt-1130652 and PFB16 Fundación Ciencia y Vida to TPA. The National Institutes of Health/National Institute of General Medical Sciences (grant RO1-GM099490) to J.E.C. The Centro Interdisciplinario de Neurociencias de Valparaíso is a Chilean Millennium Institute (P09-022-F).

Author Contributions

IEG and ADM conceived the present study; IEG and ADM designed the research; IEG, JM, OJ, RC, PO, and AP-M, JR, performed research; TP-A contributed to paper discussion and tool analysis; IEG, JCS, JEC, and ADM analyzed data; IEG, JCS, CG, JEC, and ADM wrote the paper.

SUPPLEMENTARY MATERIAL

Supplementary material is linked to the online version of the paper at http://www.nature.com/jid

REFERENCES

Anselmi F, Hernandez VH, Crispino G *et al.* (2008) ATP release through connexin hemichannels and gap junction transfer of second messengers propagate $Ca2^+$ signals across the inner ear. *Proc Natl Acad Sci USA* 105:18770–5

Arita K, Akiyama M, Aizawa T *et al.* (2006) A novel N14Y mutation in Connexin26 in keratitis-ichthyosis-deafness syndrome: analyses of altered gap junctional communication and molecular structure of N terminus of mutated Connexin26. *Am J Pathol* 169:416–23

Bargiello TA, Tang Q, Oh S *et al.* (2012) Voltage-dependent conformational changes in connexin channels. *Biochim Biophys Acta* 1818:1807–22

Barrio LC, Suchyna T, Bargiello T *et al.* (1991) Gap junctions formed by connexins 26 and 32 alone and in combination are differently affected by applied voltage. *Proc Natl Acad Sci USA* 88:8410–4

Berthoud VM, Montegna EA, Atal N *et al.* (2001) Heteromeric connexons formed by the lens connexins, connexin43 and connexin56. *Eur J Cell Biol* 80:11–9

Beyer EC, Gemel J, Martínez A *et al.* (2001) Heteromeric mixing of connexins: compatibility of partners and functional consequences. *Cell Commun Adhes* 8:199–204

Caceres-Rios H, Tamayo-Sanchez L, Duran-Mckinster C *et al.* (1996) Keratitis, ichthyosis, and deafness (KID syndrome): review of the literature and proposal of a new terminology. *Pediatr Dermatol* 13:105–13

Contreras JE, Sáez JC, Bukauskas FF *et al.* (2003) Gating and regulation of connexin 43 (Cx43) hemichannels. *Proc Natl Acad Sci USA* 100:11388–93

Contreras JE, Sánchez HA, Eugenín EA *et al.* (2002) Metabolic inhibition induces opening of unapposed connexin 43 gap junction hemichannels and reduces gap junctional communication in cortical astrocytes in culture. *Proc Natl Acad Sci USA* 99:495–500

Denda M, Inoue K, Fuziwara S *et al.* (2002) P2X purinergic receptor antagonist accelerates skin barrier repair and prevents epidermal hyperplasia induced by skin barrier disruption. *J Invest Dermatol* 119:1034–40

Djalilian AR, McGaughey D, Patel S *et al.* (2006) Connexin 26 regulates epidermal barrier and wound remodeling and promotes psoriasiform response. *J Invest Dermatol* 116:1243–53

Fiori MC, Figueroa V, Zoghbi ME *et al.* (2012) Permeation of calcium through purified connexin 26 hemichannels. *J Biol Chem* 287:40826–34

Forge A, Becker D, Casalotti S *et al.* (2003) Gap junctions in the inner ear: comparison of distribution patterns in different vertebrates and assessement of connexin composition in mammals. *J Comp Neurol* 467:207–31

Gemel J, Valiunas V, Brink PR *et al.* (2004) Connexin43 and connexin26 form gap junctions, but not heteromeric channels in co-expressing cells. *J Cell Sci* 117:2469–80

Gerido DA, DeRosa AM, Richard G *et al.* (2007) Aberrant hemichannel properties of Cx26 mutations causing skin disease and deafness. *Am J Physiol Cell Physiol* 293:C337–45

Goliger JA, Paul DL (1994) Expression of gap junction proteins Cx26, Cx31.1, Cx37, and Cx43 in developing and mature rat epidermis. *Dev Dyn* 200: 1–13

Grynkiewicz G, Poenie M, Tsien RY (1985) A new generation of Ca2+ indicators with greatly improved fluorescence properties. *J Biol Chem* 260:3440–50

Hansen DB, Braunstein TH, Nielsen MS *et al.* (2014) Distinct permeation profiles of the connexin 30 and 43 hemichannels. *FEBS Lett* 588:1446–57

Jacquemond V (1997) Indo-1 fluorescence signals elicited by membrane depolarization in enzymatically isolated mouse skeletal muscle fibers. *Biophys J* 73:920–8

Jara O, Acuna R, Garcia IE *et al.* (2012) Critical role of the first transmembrane domain of Cx26 in regulating oligomerization and function. *Mol Biol Cell* 23:3299–311

Kelsell DP, Wilgoss AL, Richard G *et al.* (2000) Connexin mutations associated with palmoplantar keratoderma and profound deafness in a single family. *Eur J Hum Genet* 8:141–4

Kwon T, Harris AL, Rossi A *et al.* (2011) Molecular dynamics simulations of the Cx26 hemichannel: evaluation of structural models with Brownian dynamics. *J Gen Physiol* 138:475–93

Kyle JW, Minogue PJ, Thomas BC *et al.* (2008) An intact connexin N-terminus is required for function but not gap junction formation. *J Cell Sci* 121:2744–50

Lagree V, Brunschwig K, Lopez P *et al.* (2003) Specific amino-acid residues in the N-terminus and TM3 implicated in channel function and oligomerization compatibility of connexin43. *J Cell Sci* 116:3189–201

Lee JR, Derosa AM, White TW (2009) Connexin mutations causing skin disease and deafness increase hemichannel activity and cell death when expressed in Xenopus oocytes. *J Invest Dermatol* 129:870–8

Levit NA, Mese G, Basaly MG *et al.* (2012) Pathological hemichannels associated with human Cx26 mutations causing Keratitis-Ichthyosis-Deafness syndrome. *Biochim Biophys Acta* 1818:2014–9

Lopez W, Gonzalez J, Liu Y *et al.* (2013a) Insights on the mechanisms of Ca(2+) regulation of connexin26 hemichannels revealed by human pathogenic mutations (D50N/Y). *J Gen Physiol* 142:23–35

Lopez W, Liu Y, Harris AL *et al.* (2013b) Divalent regulation and intersubunit interactions of human Connexin26 (Cx26) hemichannels. *Channels* 8:1–4

Maeda S, Nakagawa S, Suga M *et al.* (2009) Structure of the connexin 26 gap junction channel at 3.5A resolution. *Nature* 458:597–602

Martínez AD, Acuña R, Figueroa V *et al.* (2009) Gap-junction channels dysfunction in deafness and hearing loss. *Antioxid Redox Signal* 11:309–22

Martinez AD, Hayrapetyan V, Moreno AP *et al.* (2002) Connexin43 and connexin45 form heteromeric gap junction channels in which individual components determine permeability and regulation. *Circ Res* 90:1100–7

Martínez AD, Maripillan J, Acuna R *et al.* (2011) Different domains are critical for oligomerization compatibility of different connexins. *Biochem J* 436:35–43

Mazereeuw-Hautier J, Bitoun E, Chevrant-Breton J *et al.* (2007) Keratitis-ichthyosis-deafness syndrome: disease expression and spectrum of connexin 26 (GJB2) mutations in 14 patients. *Br J Dermatol* 156: 1015–9

Richard G (2000) Connexins: a connection with the skin. *Exp Dermatol* 9: 77–96

Richard G, Rouan F, Willoughby CE *et al.* (2002) Missense mutations in GJB2 encoding connexin-26 cause the ectodermal dysplasia keratitis-ichthyosis-deafness syndrome. *Am J Hum Genet* 70:1341–8

Risek B, Klier FG, Gilula NB (1992) Multiple gap junction genes are utilized during rat skin and hair development. *Development* 116:639–51

Rouan F, White TW, Brown N *et al.* (2001) trans-dominant inhibition of connexin-43 by mutant connexin-26: implications for dominant connexin disorders affecting epidermal differentiation. *J Cell Sci* 114:2105–13

Sáez JC, Retamal MA, Basilio D *et al.* (2005) Connexin-based gap junction hemichannels: gating mechanisms. *Biochim Biophys Acta* 1711: 215–24

Sáez JC, Schalper KA, Retamal MA *et al.* (2010) Cell membrane permeabilization via connexin hemichannels in living and dying cells. *Exp Cell Res* 316:2377–89

Salomon D, Masgrau E, Vischer S *et al.* (1994) Topography of mammalian connexins in human skin. *J Invest Dermatol* 103:240–7

Sánchez HA, Mese G, Srinivas M *et al.* (2010) Differentially altered Ca^{2+} regulation and Ca^{2+} permeability in Cx26 hemichannels formed by the A40V and G45E mutations that cause keratitis ichthyosis deafness syndrome. *J Gen Physiol* 136:47–62

Segretain D, Falk MM (2004) Regulation of connexin biosynthesis, assembly, gap junction formation, and removal. *Biochim Biophys Acta* 1662:3–21

Stout C, Goodenough DA, Paul DL (2004) Connexins: functions without junctions. *Curr Opin Cell Biol* 16:507–12

Stout CE, Costantin JL, Naus CC *et al.* (2002) Intercellular calcium signaling in astrocytes via ATP release through connexin hemichannels. *J Biol Chem* 277:10482–8

Verrall S, Hall ZW (1992) The N-terminal domains of acetylcholine receptor subunits contain recognition signals for the initial steps of receptor assembly. *Cell* 68:23–31

Verselis VK, Ginter CS, Bargiello TA (1994) Opposite voltage gating polarities of two closely related connexins. *Nature* 368:348–51

White TW, Deans MR, O'Brien J *et al.* (1999) Functional characteristics of skate connexin35, a member of the gamma subfamily of connexins expressed in the vertebrate retina. *Eur J Neurosci* 11:1883–90

Wiszniewski L, Limat A, Saurat JH *et al.* (2000) Differential expression of connexins during stratification of human keratinocytes. *J Invest Dermatol* 115:278–85